International Journal of Minerals, Metallurgy and Materials
Volume 28, Number 5, May 2021, Page 816
https://doi.org/10.1007/s12613-020-2235-5

Determining role of heterogeneous microstructure in lowering yield ratio and enhancing impact toughness in high-strength low-alloy steel

Yi-shuang Yu[1)], *Bin Hu*[1)], *Min-liang Gao*[1)], *Zhen-jia Xie*[1)], *Xue-quan Rong*[1)], *Gang Han*[1,2)], *Hui Guo*[1)], *and Cheng-jia Shang*[1,3)]

1) Collaborative Innovation Center of Steel Technology, University of Science and Technology Beijing, Beijing 100083, China
2) Institute of Advanced Materials and Technology, University of Science and Technology Beijing, Beijing 100083, China
3) State Key Laboratory of Metal Material for Marine Equipment and Application, Anshan 114021, China
(Received: 22 October 2020; revised: 29 November 2020; accepted: 2 December 2020)

Abstract: Here we present a novel approach of intercritical heat treatment for microstructure tailoring, in which intercritical annealing is introduced between conventional quenching and tempering. This induced a heterogeneous microstructure consisting of soft intercritical ferrite and hard tempered martensite, resulting in a low yield ratio (YR) and high impact toughness in a high-strength low-alloy steel. The initial yielding and subsequent work hardening behavior of the steel during tensile deformation were modified by the presence of soft intercritical ferrite after intercritical annealing, in comparison to the steel with full martensitic microstructure. The increase in YR was related to the reduction in hardness difference between the soft and hard phases due to the precipitation of nano-carbides and the recovery of dislocations during tempering. The excellent low-temperature toughness was ascribed not only to the decrease in probability of microcrack initiation for the reduction of hardness difference between two phases, but also to the increase in resistance of microcrack propagation caused by the high density of high angle grain boundaries.

Keywords: heterogeneous microstructure; yield ratio; impact toughness; intercritical heat treatment; high-strength low-alloy steel

1. Introduction

High-strength low-alloy (HSLA) steels with yield strength (YS) >690 MPa are in great demand in shipbuilding, construction, bridges, and offshore structures owing to their exceptional combination of strength and toughness, low yield ratio (YR) (ratio of YS to tensile strength), excellent weather resistance, and good weldability [1–3]. To achieve superior comprehensive properties, alloy design is very important. For example, low carbon content (<0.10wt%) is used for ensuring good weldability, Cr, Mo, and Ni for improving hardenability, microalloying elements (Nb, V, and Ti) for thermomechanical processing, and Cu for corrosion resistance and precipitation strengthening [4–5]. Traditionally, quenching and tempering (Q&T) processing is used for producing HSLA steels. Quenching is used to obtain the martensitic or bainitic microstructure for increasing the strength [6–7] while tempering improves ductility and toughness. However, the YR of HSLA steels by Q&T processing is usually higher than 0.90 [3]. How to decrease the YR became an increasingly important issue for HSLA steels with a minimum YS of 690 MPa.

Creating a heterogeneous microstructure in HSLA steels has proven to be a new method of addressing the above problem [8–11]. Heterogeneous microstructure has a significant difference in strength among different domains, generally containing a hard martensite phase embedded in the soft austenite and/or ferrite matrix [12–13], which can be fabricated by intercritical annealing [14–15]. Compared with conventional Q&T processing, intercritical annealing can markedly increase the ductility and toughness and lower the YR of low carbon low alloy steels. However, the excellent ductility and toughness comes at a loss of strength, which results from the presence of stable retained austenite induced by two-step intercritical heat treatment (intercritical annealing plus intercritical tempering) [16]. Hence, it is still a challenge to simultaneously achieve a superior balance of strength and toughness and a low YR in steels with low carbon and lean alloy.

To ensure that HSLA steels possess high strength and toughness while sustaining a low YR, a new microstructure

Corresponding authors: Hui Guo E-mail: guohui@mater.ustb.edu.cn; Cheng-jia Shang E-mail: cjshang@ustb.edu.cn

design approach, introducing intercritical annealing between the conventional Q&T processing, is proposed. Through this novel method, a heterogeneous microstructure with intercritical ferrite and tempered martensite can be achieved [17]. The microstructure would be much different compared with that in steel with two-step intercritical heat treatment for the absence of retained austenite, which means that the YR and toughening mechanism may be different. However, the effect of a heterogeneous microstructure without retained austenite on YR and toughness in HSLA steel is poorly understood to date, and requires further investigation. This study aims to explore the significance of heterogeneous microstructure, namely intercritical ferrite and martensite, on the mechanical properties of HSLA steel. To clarify the YR variation and toughening mechanism of this steel, full martensitic microstructure was also adopted for comparison with heterogeneous microstructure.

2. Experimental

The chemical composition of the experimental steel is shown in Table 1. The steel was vacuum melted and cast into a 25 kg ingot. The ingot was forged and cut into blocks of ~80 mm thickness. The blocks were then soaked at 1200°C for 120 min and hot-rolled to ~12 mm thick strips, followed by air cooling to room temperature.

Table 1. Chemical composition of experimental steel wt%

C	Si	Mn	Cr + Mo + Ni + Cu	Nb + V + Ti	B
0.09	0.21	1.43	2.66	0.15	0.0010

To prepare the heterogeneous microstructure in this steel, intercritical annealing (IA) was added between the Q&T treatments (QT), a process called intercritical heat treatment (QIAT). Fig. 1 shows the volume fraction of phases against temperature calculated using Thermo-Calc software (TCFE7 database) for the steel. The A_3 temperature (finishing temperature of ferrite-to-austenite transformation) of the experimental steel was 812°C. Between 550 and 812°C, the volume fraction of austenite increases with temperature. At 762°C, 50vol% austenite (fcc) and 50vol% ferrite (bcc) can be obtained after holding for a long time. In this work, this temperature was selected as the temperature for IA. In addition, for comparison with heterogeneous microstructure, a full martensitic structure prepared by QT was also employed in the present study. Schematics of the two heat treatments are shown in Fig. 2. After austenitizing at 900°C for 60 min, the samples were quenched in water to obtain full martensitic structure (designated as Q), and then divided into two groups. One group was tempered at 450°C for 30 min (termed as QT), the other was intercritically annealed at 760°C for 30 min and then tempered at 450°C for 30 min (referred to as QIA and QIAT, respectively).

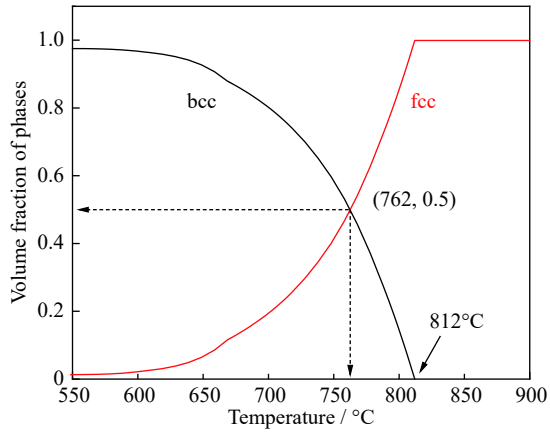

Fig. 1. Temperature–volume fraction phase diagram of the experimental steel.

After the heat treatments, tensile specimens with dimensions of ϕ5 mm × 25 mm were machined from the heat-treated strips, and the tensile axis was parallel to the transverse direction. The room-temperature tensile tests were performed on a universal testing machine (WDW-200D) equipped with an extensometer at a strain rate of 1.0 ×

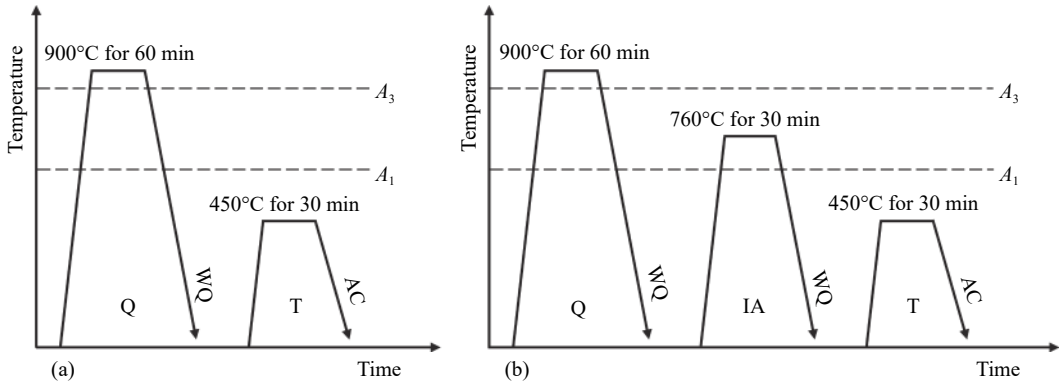

Fig. 2. Schematic diagrams illustrating two heat treatments: (a) QT; (b) QIAT (A_1 and A_3 stand for the starting and finishing temperatures of ferrite-to-austenite transformation, respectively; WQ—water quenching; AC—air cooling).

10^{-3} s^{-1}. The impact toughness in the transverse direction was measured using Charpy 45° V-notch specimens with a size of 10 mm × 10 mm × 55 mm, and Charpy impact tests were conducted at −40°C. The nanoindentation tests were carried out in displacement-controlled mode using an MTS Nano Indenter XP® system to obtain the hardness of the soft and hard phases. A constant strain rate of 0.03 s^{-1} was applied until the indenter reached a depth of 300 nm into the samples. The load was then held for 10 s before unloading, and ten measurements were made for each sample. The tests were performed on the same surface as the one used for electron backscatter diffraction (EBSD) data acquisition. Data analysis was based on the traditional Oliver–Pharr (OP) method [18].

Scanning electron microscopy (SEM) and EBSD technique were used to obtain morphology and crystallography information. The samples were mounted and mechanically polished, then etched by a 3vol% nital solution and electropolished using a solution containing 85vol% alcohol, 10vol% perchloric acid, and 5vol% glycerol for SEM and EBSD examinations. The SEM observation was made using TESCAN MIRA3 field emission scanning electron microscopy (FE-SEM) operating at 10 kV. The crystallographic data was acquired using an Oxford-EBSD system at an acceleration voltage of 20 kV and step size of 80 nm. HKL Channel 5 and MATLAB® software were employed for post-processing EBSD data. Transmission electron microscopy (TEM) samples were prepared by cutting 3 mm diameter disks from the heat-treated strips, mechanically thinning them to 60 μm, and electropolishing to perforation using a solution of 5vol% perchloric acid in ethanol at −20°C. TEM observation was conducted with an FEI Tecnai G2 F20 TEM. The volume fraction of retained austenite was determined by X-ray diffraction (XRD) using Cu K_α radiation and calculated based on the integrated intensities of (200)α, (211)α, (200)γ, (220)γ, and (311)γ diffraction peaks.

3. Results

3.1. Mechanical properties

The mechanical properties of the heat-treated samples are presented in Table 2 and Fig. 3. The Q sample exhibited tensile properties with a YS of 988 MPa, tensile strength of 1276 MPa, YR of 0.77, total elongation of 15.2%, and a −40°C impact energy of 65.0 J. After tempering at 450°C, the YS of the QT sample was increased to 1064 MPa, while the tensile strength decreased to 1141 MPa. Consequently, the YR dramatically increased to 0.93. The QT sample showed similar ductility and lower toughness with a reduction of ~52%, as compared to those in the Q sample.

When the quenched sample was subjected to IA, there was a significant change in strength, ductility, and toughness (Table 2 and Fig. 3). The yield and tensile strengths of the QIA sample were decreased to 708 and 1086 MPa respectively, thus lowering the YR. Meanwhile, uniform elongation was 6.0%, an increase of 1.9%, and total elongation was

Table 2. Mechanical properties of the studied steel after heat treatments

Processing	YS / MPa	TS / MPa	YR	UEL / %	TEL / %	CVN / J
Q	988	1276	0.77	4.1	15.2	65.0 ± 8.1
QIA	708	1086	0.65	6.0	17.0	68.5 ± 6.5
QT	1064	1141	0.93	3.7	15.0	31.5 ± 6.0
QIAT	811	958	0.85	5.3	18.2	143.5 ± 2.8

Note: YS—yield strength; TS—tensile strength; YR—yield ratio (YS/TS); UEL—uniform elongation; TEL—total elongation; CVN—Charpy V-notch impact energy.

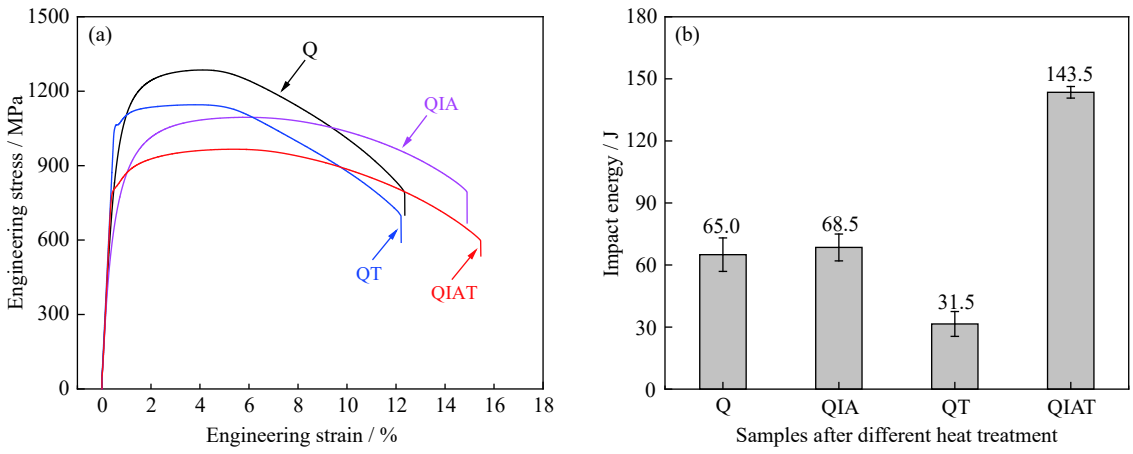

Fig. 3. Mechanical properties of experimental steels: (a) engineering stress–strain curves; (b) Charpy impact energy at −40°C.

17.0%, an increase of 1.8%, while the impact energy was slightly increased to 68.5 J. A better balance of strength and toughness was achieved in the intercritically annealed sample after tempering (Table 2 and Fig. 3). In comparison to the QIA sample, the QIAT sample showed a higher YS (811 MPa) and impact energy (143.5 J), lower tensile strength (958 MPa), and virtually the same ductility. In addition, a considerably low YR of 0.85 was obtained, which is appropriate for structural applications [19].

3.2. Microstructural characterization

The microstructure of the samples under different heat treatment conditions is shown in Fig. 4. A typical lath martensitic microstructure was observed in the Q sample (Fig. 4(a)). After IA, a heterogeneous microstructure of intercritical ferrite and martensite was obtained in the QIA sample (Fig. 4(b)). The volume fraction of intercritical ferrite was ~50vol%. The martensite can be classified into granular martensite and fibrous martensite according to its morphology. The fine granular and fibrous martensite was transformed from globular and acicular reversed austenite, respectively, during the cooling process. It is concluded that the microstructure of the QIA sample was much finer than that of the Q sample due to the transformation during cooling from the reversed austenite obtained during IA. The tempered martensite structure in the QT sample is presented in Fig. 4(c). Some of the lath boundaries were ambiguous due to the recovery of martensite, and the carbides were fine and uniformly dispersed at the boundaries and in the lath matrix. Fig. 4(d) shows the microstructure features of the QIAT sample. Fine carbides presented in the tempered matrix (intercritical ferrite and tempered martensite). The boundaries reserved were indistinct owing to the recovery of heterogeneous microstructure during tempering.

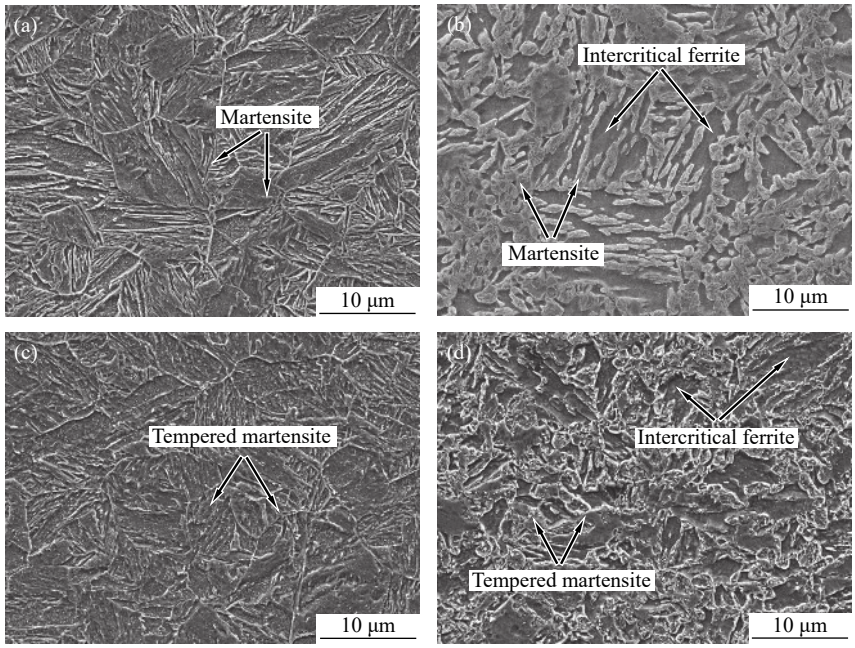

Fig. 4. SEM micrographs of (a) Q, (b) QIA, (c) QT, and (d) QIAT samples.

Fig. 5 depicts the band contrast maps showing the microstructure morphology and boundary distributions of the samples. The microstructure in the Q sample had lath morphology (Fig. 5(a)). After IA, no retained austenite was observed (Fig. 5(b)), which was consistent with the XRD result. In addition, globular and acicular reversed austenite was formed. The globular reversed austenite was nucleated at the prior austenite grain boundaries as well as the packet and block boundaries of the martensite; the acicular reversed austenite was nucleated at the block and lath boundaries [20–21]. The fine globular reversed austenite grew into one side of the adjacent two prior austenite grains (PAGs), which refined the coarse PAGs. According to the misorientation (θ), grain boundaries can be divided into three types, i.e. white ($5° < \theta < 15°$), black ($15° < \theta < 45°$), and yellow ($\theta > 45°$) lines. The density of the high angle grain boundaries (HAGBs) in the intercritically heat-treated samples was higher than that in the quenched and tempered samples, which was attributed to the refinement of microstructure.

Fig. 6 shows the Kernel average misorientation (KAM) maps analyzed by EBSD, in which the evolution of dislocation can be observed. KAM was processed based on Gaussian smoothing filter and 3rd nearest-neighbor, which represents the distribution of local dislocation density [22]. This kind of dislocation is associated with geometry-necessary dislocation. It can be seen that there is no clear decrease in the

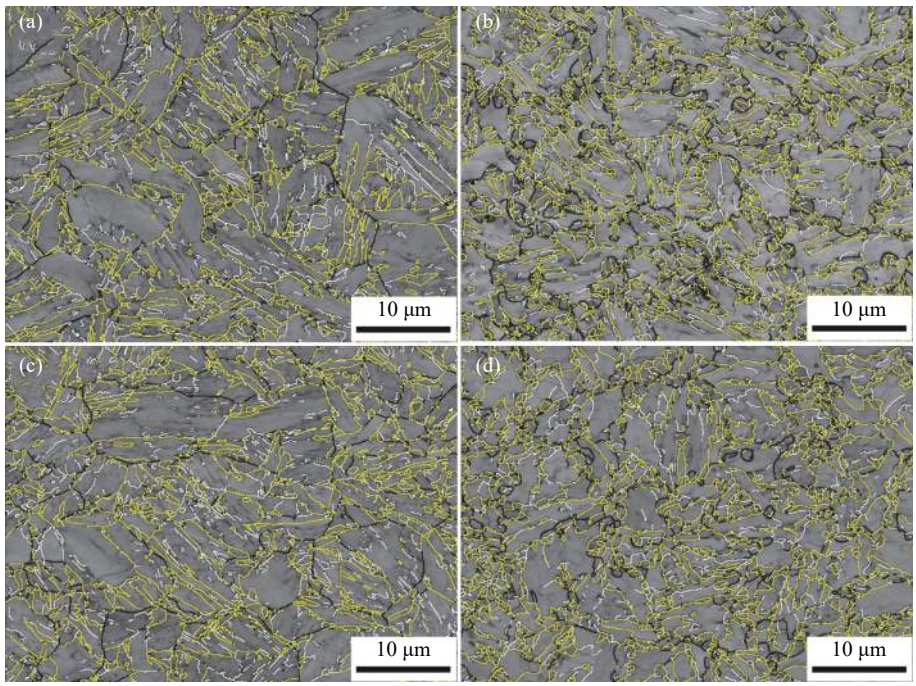

Fig. 5. Band contrast maps showing the microstructure morphology and boundary distributions of (a) Q, (b) QIA, (c) QT, and (d) QIAT samples (white line: 5° < θ < 15°, black line: 15° < θ < 45°, yellow line: θ > 45°; θ—misorientation).

distribution of KAM values of the QT sample compared to the Q sample. A remarkable KAM variation of the QIA sample was observed in the intercritical ferrite, granular martensite, and fibrous martensite, which denotes that the dislocations were heterogeneously distributed in the microstructure. In addition, the distribution of KAM in the QIAT sample was more uniform than that in the QIA sample. More specifically, the KAM values of the martensite in the QIAT sample became lower, especially in the granular martensite. This suggested that the dislocation density in granular and fibrous martensite was decreased after tempering due to its recovery.

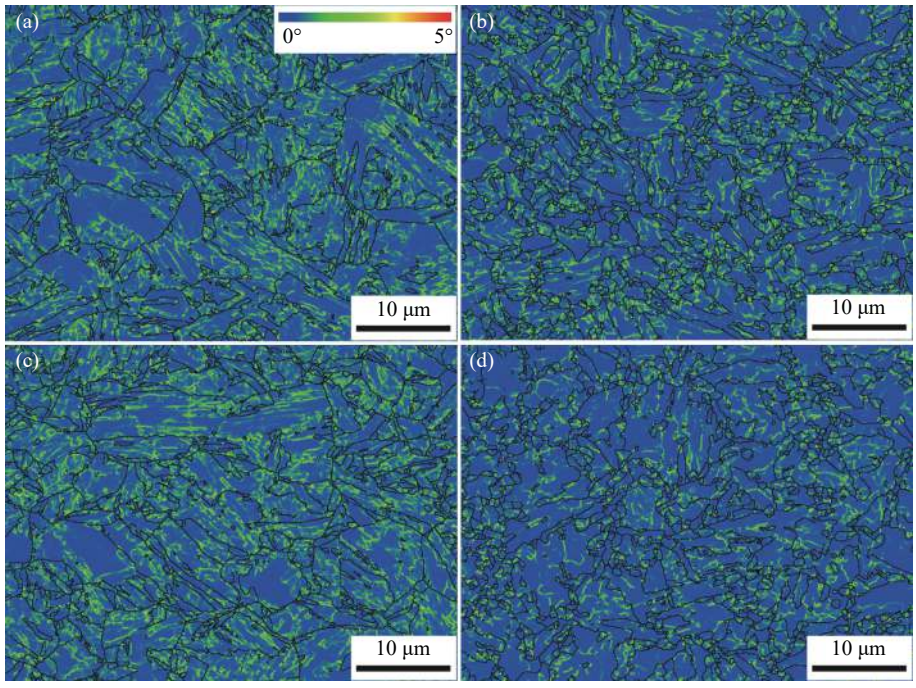

Fig. 6. Kernel average misorientation (KAM) maps of (a) Q, (b) QIA, (c) QT, and (d) QIAT samples (black line: θ > 15°, θ—misorientation).

4. Discussion

4.1. Effect of heterogeneous microstructure on strength

From the mechanical properties of samples subjected to Q&T (Table 2), the QT sample exhibited a higher YS and lower tensile strength compared with the Q sample, which resulted in a sharp increase in YR to 0.93. This was due to the microstructure recovery during tempering at 450°C. The change in YS is related to the mobility of dislocations at the early stage of plastic deformation, which determines YS [23]. During tempering, dislocation recovery, carbides precipitation, and pinning of carbides on dislocations in martensite led to higher stress to initiate dislocation motion, thus enhancing YS. Tensile strength largely relies on the strength of each phase according to the law of mixtures [24]. Therefore, the Q sample had a higher tensile strength, while the tensile strength of the QT sample was reduced due to softening during tempering. In the intercritically heat-treated condition, the QIAT sample exhibited a notable increase in YS (~14.5%) and an acceptable reduction in tensile strength (~11.8%) compared to the QIA sample. The variation in strength of the QIAT sample resulted from the precipitation of nanocarbides and the recovery of dislocation in the matrix during tempering. As a result, the YR increased to 0.85, which is still low enough for modern structural design.

To better understand the yielding behavior of the heat-treated samples, the extended Kocks–Mecking (K–M) curves [25], the instantaneous work hardening rate (Θ, $d\sigma/d\varepsilon$) against the true stress, was used in this analysis. In general, there are two stages before tensile strength is reached. One is a gradual decay of Θ caused by the anelastic reversible behavior for the bowing of matrix dislocations (Stage Ⅰ); the other is a marked transition to the plastic regime associated with the effective accumulation of dislocations during subsequent plastic deformation (Stage Ⅱ). Fig. 7 depicts the extended K–M curves of the samples. The curve of the Q sample shows an almost linear trend in Θ without visible transition from elastic to plastic regime, when the true stress exceeds 500 MPa. The microstructure of the Q sample, as mentioned above, was single quenched martensite, in which the high density of dislocations resulted in this yielding behavior. To the contrary, a noticeable transition between stage Ⅰ and stage Ⅱ, marked by a blue dot, was presented in the QT sample, which simultaneously occurred with the yielding of the sample. The yielding behavior is related to the diminishing of dislocation mobility triggered by the reduction in dislocations, the precipitation of carbides, and the pinning of the carbides on dislocations in martensite after tempering [26].

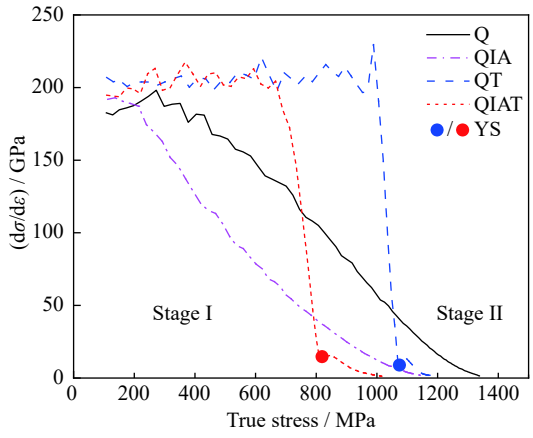

Fig. 7. Extended K–M curves of heat-treated samples (the transition marked by blue and red dots representing the yield strength (YS) of QT and QIAT samples, respectively).

In the QIA sample, a continuous decay of Θ without a notable transition was observed, which is similar to the trend in the Q sample. The absence of a clear transition from stage Ⅰ to stage Ⅱ indicated continuous yielding, which results from the heterogeneous microstructure. Owing to the presence of ~50vol% intercritical ferrite in the QIA sample, the Θ at stage Ⅰ of the extended K–M curve decreased more quickly than that at stage Ⅱ. This suggests that the intercritical ferrite yielded at a lower stress level than the martensite, and its yielding behavior was prior to that of martensite. Therefore, it is clear that the initial yielding behavior and subsequent work hardening behavior of the QIA sample during tensile deformation were modified due to the presence of intercritical ferrite as compared with the Q sample. When the intercritically annealed sample was subjected to tempering, the extended K–M curve of the QIAT sample exhibited an obvious transition from stage Ⅰ to stage Ⅱ, marked by a red dot. The sudden change in Θ was attributed to the precipitation of nanocarbides and the recovery of dislocation in the matrix during tempering.

4.2. Effect of heterogeneous microstructure on yield ratio

To further clarify the effect of strength variation on YR in the intercritically heat-treated samples, the heterogeneous microstructure was further characterized by a nanoindentation test and TEM. Fig. 8 shows the nanoindentation hardness of the intercritically annealed samples before and after tempering. It can be seen that the intercritical ferrite and martensite were the soft and hard phases, respectively. The indentation hardness of intercritical ferrite in the QIAT sample was 0.30 GPa higher than that in the QIA sample, while the indentation hardness of martensite was much lower (0.26 and 1.00 GPa reduction in fibrous martensite and granular martensite, respectively). Thus, the hardness difference between the soft intercritical ferrite and hard martensite was decreased, which was related to the tempering [27]. After tempering, the decrease in hardness of martensite was the result of the dislocation recovery and carbides precipitation. It can be inferred that the softening effect of the dislocation recovery was greater than the strengthening effect of carbides precipitation in the tempered martensite. For intercritical ferrite, the in-

creased hardness after tempering was mainly related to carbides precipitation.

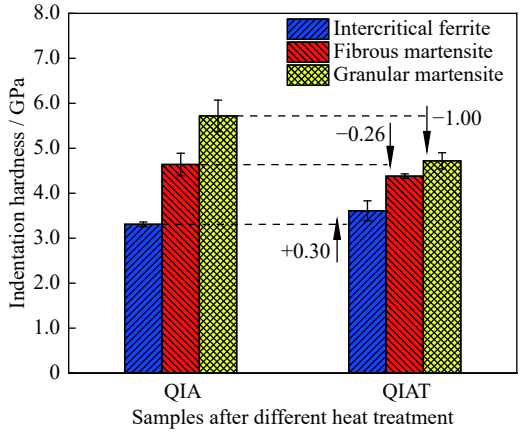

Fig. 8. Nanoindentation hardness of intercritically annealed samples before and after tempering.

TEM images showing the carbides in the intercritical ferrite of the QIA and QIAT samples are presented in Fig. 9. In the QIA sample, fine carbides with a spherical shape and a size of ~10–20 nm were distributed on dislocations in the intercritical ferrite. In contrast, a higher density of nano-carbide precipitates with a size of ~5–15 nm was observed in the QIAT sample, which contributed to the strengthening of the intercritical ferrite. Generally, the soft phase can deform first and contribute to a low YS and a high uniform elongation during deformation, while the hard phase is conducive of a high tensile strength [8,28]. Hence, the YS of the QIAT sample was increased by the precipitation strengthening in the soft intercritical ferrite, while the decrease in tensile strength is due to the reduction in indentation hardness of hard martensite caused by tempering softening. As a result, the YR increased from 0.65 to 0.85.

Swift [29] and Hollomon [30] equations indicate that YR can be expressed as a function of material constants [31]. The relationship is described as follows:

$$\mathrm{YR}=\frac{\left[b+\ln\left(1+e_{\mathrm{y}}\right)\right]^{N}}{\left(1+e_{\mathrm{y}}\right)}\frac{\exp(N-b)}{N^{N}} \tag{1}$$

where b, e_{y}, and N are additive strain constant, engineering yielding strain, and strain hardening exponent, respectively. b and N are controllable variables to determine YR. b is related to the constituent phases [9], and can be expressed as

$$b=(\alpha_{\mathrm{PF}}X_{\mathrm{PF}}+\alpha_{\mathrm{AF}}X_{\mathrm{AF}}+\alpha_{\mathrm{GB}}X_{\mathrm{GB}}+\alpha_{\mathrm{BF}}X_{\mathrm{BF}})\exp(-kX_{\mathrm{M}})+\alpha_{\mathrm{M}}X_{\mathrm{M}} \tag{2}$$

where α_i and X_i refer to the proprietary constant and volume fraction of each constituent phase, respectively, and k is the constant dependent on the size and distribution of martensite or martensite/austenite (M/A) constituent. The value of α is proposed as 0.03 for polygonal ferrite (PF), 0.015 for acicular ferrite (AF), 0.008 for granular bainite (GB), 0.003 for bainitic ferrite (BF), and 0.0003 for martensite (M) [9,31]. α tends to decrease in low-temperature transformation products with high density of dislocations, and b decreases with the fraction of phases with small α. N is complexly associated with the microstructural features such as grain size, density of dislocations, fraction of precipitates, and the amount of alloying solution.

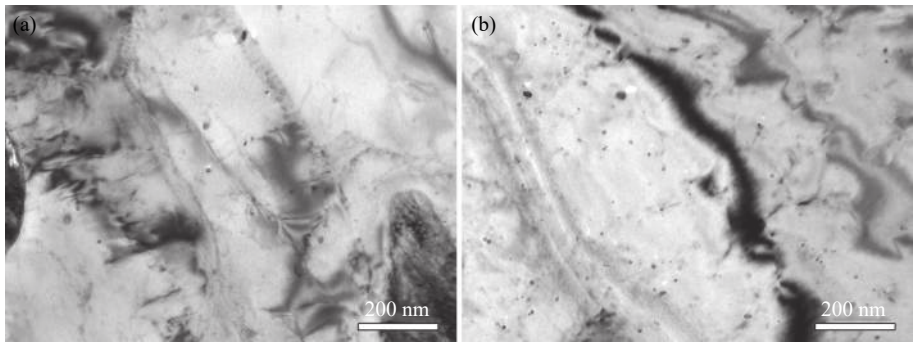

Fig. 9. TEM micrographs of nano-carbides in the intercritical ferrite of (a) QIA and (b) QIAT samples.

A previous study has shown that the YR is linearly proportional to $\ln(b/N^2)$ [31]. The YR can be reduced through microstructure modification by decreasing the b or increasing the N. Generally, the constants b and N show opposite influences on tensile properties. Increasing the volume fraction of phases like martensite would decrease the value of b and increase the YS. However, this would also decrease the value of N, which may lead to an increase in $\ln(b/N^2)$ and thus raise the YR [9]. Consequently, there exist the balanced values of b and N to satisfy the required properties with low YR. The most effective way to obtain low YR is to control the microstructure toward decreasing $\ln(b/N^2)$ by adding an appropriate proportion of soft phase into hard phase, aiming at minimizing the increase in the b value while maximizing the increase in the N value [9–10,32]. Hence, the quenched and tempered samples with full martensitic microstructure had a higher YR in this study, whereas the intercritically heat-treated samples with heterogeneous microstructure exhibited

a lower YR.

In the steel with heterogeneous microstructure, the YR is related not only to the volume fraction of soft phase, but also to the relative hardness (strength) of the soft and hard phases [8,27–28]. When the volume fraction of the soft phase is fixed, the greater the hardness difference between the soft and hard phases is, the lower the YR of the steel will be. In the intercritically annealed samples, a heterogeneous microstructure containing ~50vol% soft intercritical ferrite was achieved. After tempering, the hardness difference between the soft intercritical ferrite and hard martensite was decreased due to carbides precipitation and dislocation recovery, which led to a decrease in N value and thereby raised the YR to 0.85. In other words, the hardness difference between the soft intercritical ferrite and hard martensite was reduced, causing the increase in YR. It can be inferred that the YR of the heterogeneous microstructure can be effectively controlled by manipulating the hardness difference between the soft intercritical ferrite and the hard martensite.

4.3. Effect of heterogeneous microstructure on toughness

As is mentioned above, the samples with intercritical heat treatment exhibited higher impact energy compared to the samples with Q&T. For unraveling the toughening mechanism in the heterogeneous microstructure, the variation in grain boundaries and distribution of KAM in the samples were analyzed. The fraction and density of grain boundaries were calculated statistically based on the maps in Fig. 5, and the result is depicted in Fig. 10. The fraction of HAGBs in the QIA sample was higher compared with that in the Q sample. In addition, the fraction of HAGBs in tempered samples was increased, which resulted from the merging of lath structure with small misorientation during tempering [33]. Fig. 10(b) shows a notable difference in HAGBs density between the Q and QIA samples. The density of HAGBs in the Q and QIA samples were 1.43 and 1.77 μm^{-1}, respectively. The high density of HAGBs in the QIA sample was attributed to the refinement of microstructure. Moreover, the density of HAGBs ($15° < \theta < 45°$) in the QIA sample was much higher than that in Q sample, which means that the PAGs are much finer in the QIA sample. The HAGBs can effectively deflect or arrest microcrack propagation, thereby enhancing toughness [34]. Thus, the heterogeneous microstructure with a high density of HAGBs is the basis of toughness improvement.

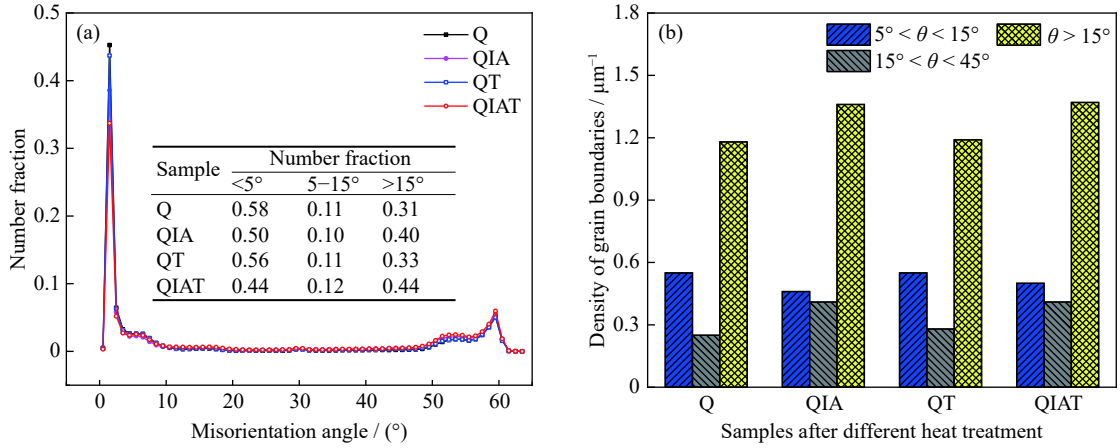

Sample	Number fraction		
	<5°	5–15°	>15°
Q	0.58	0.11	0.31
QIA	0.50	0.10	0.40
QT	0.56	0.11	0.33
QIAT	0.44	0.12	0.44

Fig. 10. Misorientation distribution (a) and boundary density (b) of heat-treated samples.

The KAM distribution of the heat-treated samples is shown in Fig. 11. The distributions of KAM in the Q and QT samples were almost the same. However, the toughness of the QT sample was lower compared to the Q sample. This may be related to the tempered martensite embrittlement. After tempering at 450°C, cementite precipitated at the PAGBs and lath boundaries, leading to intergranular or transgranular fractures [35]. The KAM distribution in the QIA sample shifted to the lower KAM zone compared to the Q sample, which means the density of dislocations was lower in the QIA sample. The toughness of the QIA sample was as low as that in the Q sample, which may be associated with the hard martensite in the heterogeneous microstructure, which can provide nucleation sites for cleavage cracks and reduce the toughness [36–37]. When the QIA sample was tempered at 450°C, a notable change in the KAM distribution was observed. The fraction of KAM between 0° and 0.65° in the QIAT sample increased, while the fraction of KAM between 0.65° and 2.00° was lower. This difference in KAM distribution between two samples may be attributed to tempering, which significantly influenced the dislocation density and low-temperature toughness. The dislocation density in martensite was decreased after tempering due to its recovery, resulting in the reduction in hardness difference between soft intercritical ferrite and hard martensite. The small hardness difference may lead to a decrease in probability of microcrack initiation, which thereby contributes to improved toughness. Consequently, it is concluded that the

higher toughness in the QIAT sample is the product of the reduction in the hardness difference caused by tempering.

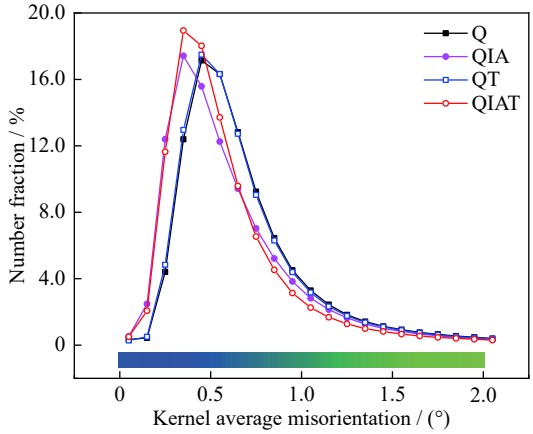

Fig. 11. KAM distribution of heat-treated samples.

According to this analysis, the superior toughness in the QIAT sample was related to the reduction in hardness difference between the soft and hard phases and the high density of HAGBs. In other words, the exceptional toughness of the samples with intercritical heat treatment was attributed to "double effects". One effect is the decrease in the probability of microcrack initiation for the reduction in hardness difference, the other is the effective deflection or arrest of microcrack propagation induced by the high density of HAGBs.

5. Conclusions

A novel intercritical heat treatment was carried out in a HSLA steel to obtain heterogeneous microstructure with low yield ratio and high impact toughness. The microstructure and mechanical properties of this steel were characterized and compared to those of steel treated by conventional quenching and tempering treatment. The main conclusions are summarized as follows.

(1) A heterogeneous microstructure consisting of soft intercritical ferrite and hard tempered martensite was obtained in the studied steel by introducing intercritical annealing between the quenching and tempering. The structure was much finer than full martensitic microstructure.

(2) Compared to the steel with full martensitic microstructure, the initial yielding behavior and subsequent work hardening behavior of the steel during tensile deformation were modified by the presence of soft intercritical ferrite after intercritical annealing. Hence, a low yield strength of 708 MPa, a high total elongation of 17.0%, and a low yield ratio of 0.65 were obtained. After tempering, the hardness difference between the soft intercritical ferrite and hard martensite was decreased due to the precipitation of nano-carbides and the recovery of dislocations, which in turn contributed to a yield strength increment of 103 MPa. At the same time, the yield ratio was increased to 0.85, which is still low enough for structural applications.

(3) The average Charpy impact energy at −40°C of the intercritically annealed samples before and after tempering was 68.5 and 143.5 J respectively, both of which are clearly higher than the 31.5 J of the quenched and tempered samples. The excellent toughness of the quenched, intercritically annealed, and tempered samples was attributed to the reasonably small hardness difference between the soft and hard phases and the high density of high angle grain boundaries. These, in turn, contributed to decreasing the probability of microcrack initiation and increasing the resistance of microcrack propagation, thus enhancing the impact toughness.

Acknowledgements

This work was financially supported by the National Key Research and Development Program of China (No. 2017YFB 0304800). One of the authors, H. Guo, would like to express her gratitude for the financial support of China Scholarship Council (award for one year visiting at Northwestern University in the USA, No. 201706465056).

References

[1] Y.Q. Weng, C.F. Yang, and C.J. Shang, State-of-the-art and development trends of HSLA steels in China, *Iron Steel*, 46(2011), No. 9, p. 1.

[2] D.S. Liu, B.G. Cheng, and Y.Y. Chen, Strengthening and toughening of a heavy plate steel for shipbuilding with yield strength of approximately 690 MPa, *Metall. Mater. Trans. A*, 44(2013), No. 1, p. 440.

[3] S.K. Dhua, A. Ray, and D.S. Sarma, Effect of tempering temperatures on the mechanical properties and microstructures of HSLA-100 type copper-bearing steels, *Mater. Sci. Eng. A*, 318(2001), No. 1-2, p. 197.

[4] M.J. Sohrabi, H. Mirzadeh, M.S. Mehranpour, A. Heydarinia, and R. Razi, Aging kinetics and mechanical properties of copper-bearing low-carbon HSLA-100 microalloyed steel, *Arch. Civ. Mech. Eng.*, 19(2019), No. 4, p. 1409.

[5] S.T. Wang, S.W. Yang, K.W. Gao, and X.L. He, Corrosion behavior and corrosion products of a low-alloy weathering steel in Qingdao and Wanning, *Int. J. Miner. Metall. Mater.*, 16(2009), No. 1, p. 58.

[6] Y.J. Zhao, X.P. Ren, W.C. Yang, and Y. Zang, Design of a low-alloy high-strength and high-toughness martensitic steel, *Int. J. Miner. Metall. Mater.*, 20(2013), No. 8, p. 733.

[7] G. Krauss, Tempering of lath martensite in low and medium carbon steels: assessment and challenges, *Steel Res. Int.*, 88(2017), No. 10, art. No. 1700038.

[8] C.J. Tang, S.L. Liu, and C.J. Shang, Micromechanical behavior and failure mechanism of F/B multi-phase high performance steel, *J. Iron Steel Res. Int.*, 23(2016), No. 5, p. 489.

[9] Y.M. Kim, S.K. Kim, and N.J. Kim, Simple method for tailoring the optimum microstructures of high-strength low-alloyed steels by the use of constitutive equation, *Mater. Sci. Eng. A*, 743(2019), p. 138.

[10] X.H. Li, Y.C. Liu, K.F. Gan, J. Dong, and C.X. Liu, Acquiring

a low yield ratio well synchronized with enhanced strength of HSLA pipeline steels through adjusting multiple-phase microstructures, *Mater. Sci. Eng. A*, 785(2020), art. No. 139350.

[11] W.S. Li, H.Y. Gao, Z.Y. Li, H. Nakashima, S. Hata, and W.H. Tian, Effect of lower bainite/martensite/retained austenite triplex microstructure on the mechanical properties of a low-carbon steel with quenching and partitioning process, *Int. J. Miner. Metall. Mater.*, 23(2016), No. 3, p. 303.

[12] X.L. Wu and Y.T. Zhu, Heterogeneous materials: A new class of materials with unprecedented mechanical properties, *Mater. Res. Lett.*, 5(2017), No. 8, p. 527.

[13] B. Gao, X.F. Chen, Z.Y. Pan, J.S. Li, Y. Ma, Y. Cao, M.P. Liu, Q.Q. Lai, L.R. Xiao, and H. Zhou, A high-strength heterogeneous structural dual-phase steel, *J. Mater. Sci.*, 54(2019), p. 12898.

[14] Z.J. Xie, C.J. Shang, X.L. Wang, X.M. Wang, G. Han, and R.D.K. Misra, Recent progress in third-generation low alloy steels developed under M^3 microstructure control, *Int. J. Miner. Metall. Mater.*, 27(2020), No. 1, p. 1.

[15] Z.J. Xie, G. Han, Y.S. Yu, C.J. Shang, and R.D.K. Misra, The determining role of intercritical annealing condition on retained austenite and mechanical properties of a low carbon steel: Experimental and theoretical analysis, *Mater. Charact.*, 153(2019), p. 208.

[16] Z.J. Xie, S.F. Yuan, W.H. Zhou, J.R. Yang, H. Guo, and C.J. Shang, Stabilization of retained austenite by the two-step intercritical heat treatment and its effect on the toughness of a low alloyed steel, *Mater. Des.*, 59(2014), p. 193.

[17] B.G. Cheng, M. Luo, and D.S. Liu, High strength, low carbon, Cu containing steel plates with tailored microstructure and low yield ratio, *Ironmaking Steelmaking*, 42(2015), No. 8, p. 608.

[18] W.C. Oliver and G.M. Pharr, An improved technique for determining hardness and elastic modulus using load and displacement sensing indentation experiments, *J. Mater. Res.*, 7(1992), No. 6, p. 1564.

[19] Y.M. Kim, S.K. Kim, Y.J. Lim, and N.J. Kim, Effect of microstructure on the yield ratio and low temperature toughness of linepipe steels, *ISIJ Int.*, 42(2002), No. 12, p. 1571.

[20] X.G. Zhang, G. Miyamoto, Y. Toji, S. Nambu, T. Koseki, and T. Furuhara, Orientation of austenite reverted from martensite in Fe–2Mn–1.5Si–0.3C alloy, *Acta Mater.*, 144(2018), p. 601.

[21] S.F. Yuan, Z.J. Xie, J.L. Wang, L.H. Zhu, L. Yan, C.J. Shang, and R.D.K. Misra, Effect of heterogeneous microstructure on refining austenite grain size in low alloy heavy-gage plate, *Metals*, 10(2020), No. 1, p. 132.

[22] M. Calcagnotto, D. Ponge, E. Demir, and D. Raabe, Orientation gradients and geometrically necessary dislocations in ultrafine grained dual-phase steels studied by 2D and 3D EBSD, *Mater. Sci. Eng. A*, 527(2010), No. 10-11, p. 2738.

[23] V. Vitek and F. Kroupa, Dislocation theory of slip geometry and temperature dependence of flow stress in BCC metals, *Phys. Status Solidi B*, 18(1966), No. 2, p. 703.

[24] A. Bag and K.K. Ray, A new model to explain the unusual tensile behavior of high martensite dual-phase steels, *Metall. Mater. Trans. A*, 32(2001), No. 9, p. 2400.

[25] U.F. Kocks and H. Mecking, Physics and phenomenology of strain hardening: The FCC case, *Prog. Mater Sci.*, 48(2003), No. 3, p. 171.

[26] G. Krauss, *Steels*: *Processing*, *Structure*, *and Performance*, 2nd ed., ASM International, Ohio, 2015, p. 373.

[27] C.Y. Chen, C.H. Li, T.C. Tsao, P.H. Chiu, S.P. Tsai, J.R. Yang, L.J. Chiang, and S.H. Wang, A novel technique for developing a dual-phase steel with a lower strength difference between ferrite and martensite, *Mater. Today Commun.*, 23(2020), art. No. 100895.

[28] C.J. Tang, C.J. Shang, S.L. Liu, H.L. Guan, R.D.K. Misra, and Y.B. Chen, Effect of volume fraction of bainite on strain hardening behavior and deformation mechanism of F/B multiphase steel, *Mater. Sci. Eng. A*, 731(2018), p. 173.

[29] H.W. Swift, Plastic instability under plane stress, *J. Mech. Phys. Solids*, 1(1952), No. 1, p. 1.

[30] J.H. Hollomon, Tensile deformation, *Trans. Met. Soc. AIME*, 162(1945), p. 268.

[31] S.K. Kim, Y.M. Kim, Y.J. Lim, and N.J. Kim, Relationship between yield ratio and the material constants of the Swift equation, *Met. Mater. Int.*, 12(2006), No. 2, art. No. 131.

[32] Y.C. Liu, L. Shi, C.X. Liu, L.M. Yu, Z.S. Yan, and H.J. Li, Effect of step quenching on microstructures and mechanical properties of HSLA steel, *Mater. Sci. Eng. A*, 675(2016), p. 371.

[33] G.H. Gao, H. Zhang, and B.Z. Bai, Effect of tempering temperature on low temperature impact toughness of a low carbon Mn-series bainitic steel, *Acta Metall. Sin.*, 47(2011), No. 5, p. 513.

[34] B.B. Wu, Z.Q. Wang, X.L. Wang, W.S. Xu, C.J. Shang, and R.D.K. Misra, Toughening of martensite matrix in high strength low alloy steel: Regulation of variant pairs, *Mater. Sci. Eng. A*, 759(2019), p. 430.

[35] B.B. Wu, H. Chen, C.J. Shang, K.Y. Xie, and R.D.K. Misra, Effect of tempering mode on the microstructure and mechanical properties of a lean alloy martensitic steel: Conventional reheating versus induction reheating, *J. Mater. Eng. Perform.*, 28(2019), p. 2807.

[36] X.D. Li, Y.R. Fan, X.P. Ma, S.V. Subramanian, and C.J. Shang, Influence of martensite–austenite constituents formed at different intercritical temperatures on toughness, *Mater. Des.*, 67(2015), p. 457.

[37] X.D. Li, C.J. Shang, X.P. Ma, B. Gault, S.V. Subramanian, J.B. Sun, and R.D.K. Misra, Elemental distribution in the martensite–austenite constituent in intercritically reheated coarse-grained heat-affected zone of a high-strength pipeline steel, *Scripta Mater.*, 139(2017), p. 67.